J Solid State Electrochem (2011) 15:357–366
DOI 10.1007/s10008-010-1274-7

ORIGINAL PAPER

# On the role of lattice dynamics on low-temperature oxygen mobility in solid oxides: a neutron diffraction and first-principles investigation of $La_2CuO_{4+\delta}$

**Antoine Villesuzanne · Werner Paulus · Alain Cousson · Shoichi Hosoya · Loïc Le Dréau · Olivier Hernandez · Carmelo Prestipino · Mohamed Ikbel Houchati · Juerg Schefer**

Received: 30 October 2010 / Revised: 8 November 2010 / Accepted: 9 November 2010 / Published online: 30 December 2010


**Abstract** The structure of oxygen-intercalated $La_2CuO_{4.07}$ has been investigated at 20 and 300 K by neutron diffraction on an electrochemically oxidized single crystal. At 20 K, reconstruction of the nuclear density by maximum entropy method shows strong displacements of the apical oxygen atoms towards [100] with respect to the *F*-centred unit cell, whilst displacements towards [110] and [100] were both found to be present at ambient temperature. Combining structural studies with first-principles lattice dynamical calculations, we interpret the displacements of the apical oxygen atoms to be at least partially of dynamic origin already at ambient temperature. Strong displacements of the apical oxygen atoms of stoichiometric and oxygen-doped $La_2CuO_{4+\delta}$ and corresponding associated lattice instabilities, i.e. low-energy phonon modes, are considered as a general prerequisite of low-temperature oxygen diffusion mechanisms. Lattice dynamical calculations on $La_2CuO_{4+\delta}$ suggest that the oxygen species diffusing at low temperature are not the interstitial but, more prominently, the apical oxygen atoms. The presence of interstitial oxygen atoms is, however, important to amplify via specific, low-energy phonon modes, a dynamic exchange mechanism between apical and vacant interstitial oxygen sites, thus allowing a dynamically triggered, shallow potential oxygen diffusion pathway. The crucial role of lattice dynamics to enable low-temperature oxygen mobility in $K_2NiF_4$-type oxides is discussed on a microscopic scale and compared to similar low-temperature oxygen diffusion mechanisms, recently proposed for non-stoichiometric oxides with Brownmillerite-type structure.

**Keywords** Oxygen mobility · Non-stoichiometry · Neutron diffraction · Lattice dynamics · Density functional theory · Ruddlesden–Popper series

Dedicated to Prof. R. Schöllhorn on his 75th birthday.

A. Villesuzanne
CNRS, University of Bordeaux, ICMCB,
87 Av. Dr. A. Schweitzer,
33608 Pessac Cedex, France

W. Paulus (✉) · L. Le Dréau · O. Hernandez · C. Prestipino · M. Ikbel Houchati
University of Rennes 1, Sciences Chimiques de Rennes UMR CNRS 6226, Campus de Beaulieu,
Bâtiment 10B,
35042 Rennes Cedex, France
e-mail: werner.paulus@univ-rennes1.fr

A. Cousson
Laboratoire Léon Brillouin, CEA-CNRS, CEN Saclay,
F91191 Gif-sur-Yvette, France

S. Hosoya
Center for Crystal Science & Technology,
University of Yamanashi,
7 Miyamae,
Kofu 400-8511, Japan

L. Le Dréau · J. Schefer
Paul Scherrer Institut, Laboratory for Neutron Scattering,
CH-5232 Villigen, Switzerland

## Introduction

The origin of low-temperature oxygen mobility in non-stoichiometric oxides is of fundamental interest for the development of technologically important devices as oxygen sensors, oxygen membranes or electrolytes operat-

ing in solid oxide fuel cells. Oxygen has been proven to be mobile in several oxides already at room temperature; the most important stoichiometric changes obtained by electrochemical intercalation reactions have been obtained for oxides with Brownmillerite-type structure, e.g. $Sr(Fe,Co)O_{2.5}$, which can be easily oxidized to the cubic $Sr(Fe,Co)O_3$, thereby forming several intermediate phases with complex oxygen ordering [1–3]. Oxygen intercalation into Brownmillerite-type frameworks is equivalent to the filling up of the empty 1D oxygen vacancy channels, i.e. the uptake of oxygen on vacant lattice sites. Another family of compounds, showing low-temperature oxygen mobility, belongs to the $K_2NiF_4$ structure type such as $La_2MO_4$ (M = Cu, Ni, Co) [4–6]. For the latter systems, oxygen is no longer intercalated on regular vacancy but on interstitial vacancy lattice sites, yielding a principal difference concerning the underlying diffusion mechanism and pathway.

The hopping mechanism of oxygen diffusion/intercalation in Brownmillerite-type oxides has recently been interpreted to essentially rely on distinct low-energy phonon modes, able to overcome the necessary activation energy for site diffusion (typically described in the classical Arrhenius-type thermally activated hopping, including a temperature-dependent activation energy) [7]. An important prerequisite for this phonon-assisted diffusion mechanism is the presence of a shallow potential for mobile oxygen atoms, allowing an easy move of this unstable position along the underlying framework via vacant regular or interstitial lattice sites. The aim of this work was to underline the more general aspect of this new diffusion mechanism, which proved to be essential in the Brownmillerite frameworks with regular 1D oxygen vacancy channels, towards compounds with the $K_2NiF_4$ structure type and, namely, for $La_2CuO_4$ which can be reversibly oxidized by electrochemical methods at room temperature to $La_2CuO_{4.07}$ in an aqueous alkaline electrolyte [5]. The diffusion pathway and associated changes in the valence states of the interstitial and diffusing oxygen atoms are still debated in the literature. We will here focus on correlating high-quality neutron structure analysis carried out on a $La_2CuO_{4.07}$ single crystal at 300 and 20 K, together with phonon mode calculations, in order to underline the importance of lattice dynamics for the oxygen diffusion mechanism, already at room temperature.

## Experimental

$La_2CuO_4$ single crystals were grown by the travelling solvent floating zone technique. Details of the synthesis have been described elsewhere [8]. The measured crystal had dimensions of about $3\times3\times2$ mm$^3$ and was electrochemically oxidized in a 1 N KOH electrolyte at ambient temperature. The applied current was chosen to be 50 μA, which would have been theoretically sufficient to oxidize the whole crystal up to $La_2CuO_{4.07}$ in less than 1 day. Due to the strongly reduced reaction kinetics of the single crystal compared to a polycrystalline sample, electrochemical oxidation required about 1 year to achieve the maximum oxygen doping.

Neutron diffraction experiments have been carried out on the 5C2 four-circle diffractometer, installed at the ORPHEE reactor, Laboratoire Léon Brillouin, CEA/Saclay, France. The wavelength used was 0.831(1) Å; complete data collection of $\pm h,k,l$ has been recorded up to 0.94 Å$^{-1}$ in $\sin\theta/\lambda$. The crystal has been determined to be two times twinned, resulting into four twin domains as outlined in [4]. Least-squares structure refinement has been carried out using SHELX 97 [9]; subsequently, the as-phased data were used for the reconstruction of the nuclear densities by the maximum entropy method using the package MEED developed by Kumazawa et al. [10]. Scattering lengths used for La, Cu and O were 8.24, 7.718 and 5.805 fm, respectively, as given in the neutron scattering tables from Koester et al. [11].

Phonon frequencies and lattice relaxation for $La_2CuO_{4+\delta}$ were calculated from first principles within density functional theory (DFT) as implemented in the pseudopotential code VASP [12–14]. Projected augmented wave potentials were used to describe ionic core–valence interactions, and the generalized gradient approximation by Perdew et al. [15] was used for the exchange–correlation potential. For the sake of comparison, calculations were done in a *F*4/*mmm* tetragonal unit cell derived from the experimental structural data at room temperature ($Z$=4, Table 1) for both stoichiometric $La_2CuO_4$ and for one interstitial oxygen atom per unit cell, corresponding to $La_2CuO_{4.25}$. In the latter case, the number of electrons was adjusted (associated to a background charge) so as to correspond formally to $\delta$=1/16 in $La_2CuO_{4+\delta}$, and all atomic positions were relaxed with fixed unit cell parameters.

## Results and discussion: neutron diffraction

The as-grown $La_2CuO_{4.00}$ single crystal showed the typical superstructure reflections related to the orthorhombic symmetry with space group *Bmab*. Due to the phase transition from the high-temperature tetragonal (parent phase in *I*4/*mmm*) to the low-temperature orthorhombic phase with *Bmab* space group, the single crystal exhibits the presence of pseudo-merohedral twinning, yielding four twin individuals of about equal volume fraction. Twinning is principally a problem for structure refinement; for the given system, it implies a (not perfect) coincidence of the *a*- and *b*-axes, resulting in a partial superimposition of (*hkl*) and (*khl*) reflections from the different twin individuals. During electrochemical oxidation, the crystal was checked *ex situ* several times by neutron diffraction on completeness

**Table 1** Structural data of a two times twinned (four twin individuals) $La_2CuO_{4.07}$ crystal at room temperature (first line) and 20 K (second line) in *F4/mmm*

| Atom | *x* | *y* | *z* | Occup. factor | $U_{11}$ | $U_{22}$ | $U_{33}$ | $U_{12}$ | $U_{eq}$ |
|---|---|---|---|---|---|---|---|---|---|
| La | 0 | 0 | 0.3604(1) | 0.1225(12) | 0.0097(2) | 0.0097(2) | 0.0069(2) | | 0.0088(2) |
| | | | 0.3604(1) | 0.1224(24) | 0.0056(3) | 0.0056(3) | 0.0036(4) | | 0.0049(3) |
| Cu | 0 | 0 | 0 | 0.0625 | 0.0047(2) | 0.0047(2) | 0.0126(3) | | 0.0073(2) |
| | 0 | 0 | 0 | 0.0625 | 0.0025(4) | 0.0025(4) | 0.0079(7) | | 0.0043(4) |
| $O_{ap}$ | 0 | 0 | 0.1822(1) | 0.1140(17) | 0.0302(6) | 0.0302(6) | 0.0074(4) | | 0.0226(4) |
| | | | 0.1823(2) | 0.1184(33) | 0.0265(10) | 0.0265(10) | 0.0058(9) | | 0.0196(8) |
| $O_{eq}$ | ¼ | ¼ | 0 | 0.1236(17) | 0.0074(2) | 0.0074(2) | 0.0212(4) | −0.0017(2) | 0.0120(2) |
| | | | | 0.1228(30) | 0.0041(5) | 0.0041(5) | 0.0167(8) | −0.0011(5) | 0.0083(5) |
| $O_{int}$ | ¼ | ¼ | ¼ | 0.0063(14) | 0.028(9) | | | | |
| | | | | 0.0053(20) | 0.011(106) | | | | |

Complete data sets up to 0.94 $\sin\Theta/\lambda$ $Å^{-1}$ have been taken into account (each reflection up to six times eq.). Displacement parameters $U_{ij}$ are given in $Å^2$

Room temperature: space group *F4/mmm*, $a$=5.35(1) Å, $b$=5.41(1) Å, $c$=13.24(3) Å; reflection range: $-11\le h\le 5$, $-7\le k\le 11$, $-27\le l\le 19$, max. $2-\theta$=102.67°, $\lambda$=0.831(1) Å; $R_{int}$=2.39%, $R(F^2)$=6.52%, $R(F)$=2.61%, g.o.f.=1.26, 834 total and 323 independent reflections

20 K: space group *F4/mmm*, $a$=5.34(1) Å, $b$=5.38(1) Å, $c$=13.20(3) Å; reflection range: $-10\le h\le 10$, $-7\le k\le 9$, $-22\le l\le 22$, max. $2-\theta$=102.4°, $\lambda$=0.831(1) Å; $R_{int}$=3.74%, $R(F^2)$=8.20%, $R(F)$=3.30%, g.o.f.=1.42, 670 total and 371 independent reflections

of oxidation. We used the twinning and related separation of (*hh*0) reflections to easily access the orthorhombicity [4], directly indicating the evolution of oxygen stoichiometry. For a crystal oriented with the *c*-axis perpendicular to the diffraction plane of the diffractometer, the splitting Δ between (*hh*0)-type reflections of different twin individuals obtained by a transversal scan (omega scan) is given by Δ= arctan ($a/b$) − arctan ($b/a$). The evolution of lattice parameters has already been previously studied by *in situ* neutron powder diffraction in [5]. From this study, we can directly access the evolution of the orthorhombicity with $\delta$. For the stoichiometric $La_2CuO_{4.00}$ single crystal, Δ is expected to be 0.48°, increasing to Δ=0.79° for the fully oxidized $La_2CuO_{4.07}$ phase. The intermediate phase $La_2CuO_{4.03}$ shows, however, a reduced orthorhombicity with an expected Δ of 0.33° only [5]. We followed the orthorhombicity of the electrochemically oxidized single crystal, measuring the splitting of the (220) reflections. Moreover, we followed the intensity of the strongest superstructure reflections such as the (504) reflection, which is no longer observed for the oxidized phase, in order to monitor the completeness of transformation towards the $La_2CuO_{4.07}$ *Fmmm* phase.

Since the oxidation of the crystal took about 1 year to complete, one would expect that the reaction front proceeds from the outer part of the crystal towards the inner part, creating an inhomogeneous crystal containing oxidized and reduced parts at the same time. However, the measured evolution of orthorhombicity is in perfect agreement with the aforementioned expected changes of the splitting Δ, and no significant increase of reflection width has been detected during the whole oxidation period. Taking into account the elevated current applied, these findings are astonishing as they imply a homogeneous distribution of the extra oxygen all over the crystal along the whole intercalation reaction.

After the completion of electrochemical oxidation reaction, complete data collections have been recorded at room temperature and 20 K and the structural model was successively refined by least-squares method. The results are graphically represented in Fig. 1 and quantified in Table 1. The uptake of oxygen atoms is accompanied by a loss of the 3D long-range order passing from stoichiometric $La_2CuO_{4.00}$ with space group *Bmab* to $La_2CuO_{4+\delta}$ showing an average *Fmmm* symmetry, as observed with X-ray and neutron powder diffraction [5].

As a result of the twinning, (*hkl*) and (*khl*) reflections are mixed up, and, as found analysing their intensities, show an almost equal distribution of the volume fractions of the four twin individuals. Consequently, structure refinements have been undertaken in the average symmetry *F4/mmm* in spite of the real symmetry being still orthorhombic. The low reliability factors for averaging equivalent reflections is $R_{eq}$= 2.39% in *F4/mmm* and $R_{eq}$=1.68% in *Fmmm* at ambient temperature, confirming the presence of two almost equivalent volume fractions of the twin individuals. A respective loss of superstructure reflection intensities has also been found when oxidizing stoichiometric, orthorhombic $La_2NiO_{4.00}$ to $La_2NiO_{4+\delta}$, with tetragonal symmetry and space group *F4/mmm* [4], whereas $La_2CoO_{4+\delta}$ shows, as the homologous copper phase, always an orthorhombic symmetry, independent of $\delta$ up to ≈0.25 [6].

The structure obtained for the refinement in *F4/mmm* gives an averaged view only, imposed by the twinning and

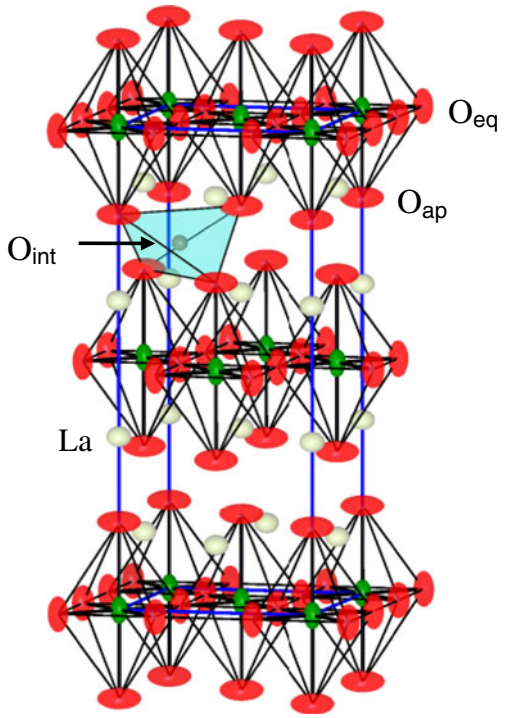


**Fig. 1** Structure scheme of $La_2CuO_{4+\delta}$ showing the strong anisotropic displacement factors, essentially for the oxygen atoms. Whilst the anisotropic elongations for the equatorial oxygen atoms are along the *c*-axis, strong discus-like distributions are found for the apical oxygen atoms in the *a*,*b* plane. One interstitial oxygen atom is outlined for the non-distorted structure, resulting in $O_{ap}$–$O_{int}$ distances of about 2.1 Å only. As outlined in the text, this $O_{int}(O_{ap})_4$ tetrahedra is symmetrically enlarged, resulting in $O_{ap}$–$O_{int}$ distances of 2.58 Å, indicating a normal $O^{2-}$ valence state for the interstitial oxygen atoms

the loss of the superstructure reflections. Strong anisotropic displacement parameters for both apical and equatorial oxygen atoms are obtained, indicating pronounced static and/or dynamic displacements (see Table 1). The interstitial oxygen ($O_{int}$) was found, analogously to the homologous Ni phase, to be located exactly on the ¼, ¼, ¼ site, coordinated by four apical oxygen atoms, as represented in Fig. 1. For $T$=293 and 20 K, the refinement converged for the interstitial oxygen stoichiometry to be equivalent to $\delta$=0.10(2) and 0.11(2), respectively. We want to stress here that despite the high quality of the diffraction data, a quantitative analysis of the interstitial oxygen atoms in terms of site occupation and displacement behaviour is not as evident due to the small amount of oxygen intercalated. From electrochemical investigations carried out in a galvanostatic mode, we know that $\delta\approx0.07$ is the maximum amount possible of interstitial oxygen atoms [5]. The value of $\delta$=0.07 corresponds to an extra oxygen occupation of 0.28/unit cell, referenced for the *F* cell containing four formula units. This means that only one interstitial oxygen atom is present for about four unit cells.

During the refinement, all atomic occupancy factors were set to be free (apart from the copper atom which was fixed to full site occupancy), as well as anisotropic displacement parameters, except for the interstitial oxygen atom which was refined isotropically. This approach allows describing a full occupation of the equatorial oxygen atom, whilst only 91% of the scattering density of the apical oxygen atoms was found. This implies that the disorder of the apical oxygen atom is quite complex and probably needs to be described anharmonically, also because we were unable to localize from the Fourier calculations any additional corresponding densities.

Strong oxygen disorder has also been found for the Ni and Co homologous phases, but the key question in the context of low-temperature oxygen mobility is to know whether this disorder is of static or dynamic origin. Whereas the displacement factors for La and Cu decrease considerably from ambient temperature down to 20 K (Table 1), the displacement factors of the oxygen atoms do not follow the same trend. This indicates that the strong anisotropic values are, at least at low temperatures, mainly related to important static displacements. In order to obtain more insight towards a real structure approach, we subjected the phased data from the as-obtained refinements to a reconstruction of the nuclear scattering density by the maximum entropy method (MEM). MEM allows a model-free reconstruction of anharmonic displacement factors, the only constraint being imposed by the symmetry of the underlying space group, i.e. *F*4/*mmm*.

MEM reconstruction shows a more detailed view of the oxygen disorder, specifically concerning the apical oxygen atoms. Whilst it confirms the strong disorder scenario in the *a*–*b* plane (top part of Fig. 2), additional densities are found close to the average position of the apical oxygen atoms. At 20 K, this density is limited to maxima pointing towards the [100] directions with respect to the *F*-centred unit cell, whilst at ambient temperature, densities along [100] and [110] are simultaneously present. We interpret the densities along [100] at 20 K as a fraction of the apical oxygen atoms which are pushed away from the average position by sterical effects induced by the presence of interstitial oxygen atoms. These local distortions go along with changes of the $O_{int}$–$O_{ap}$ distance from 2.10 Å to about 2.58 Å or, in terms of the tilt angle of the $CuO_6$ octahedra, from about 4° found for the stoichiometric $La_2CuO_{4.00}$ phase at ambient temperature to 12° for the oxygen-doped phase. The distance of 2.58 Å is quite reasonable, taking into account the normal valence state of $O^{2-}$. This is in contradiction to findings coming out from theoretical investigations [16] whereby the existence of $O^{-1}$ is claimed. However, in [16], no structural relaxation was allowed to a model derived from $La_2CuO_{4.032}$ structural data (samples with negligible amount of interstitial oxygen), leading thus to drastically short $O_{int}$–$O_{ap}$ bonds.

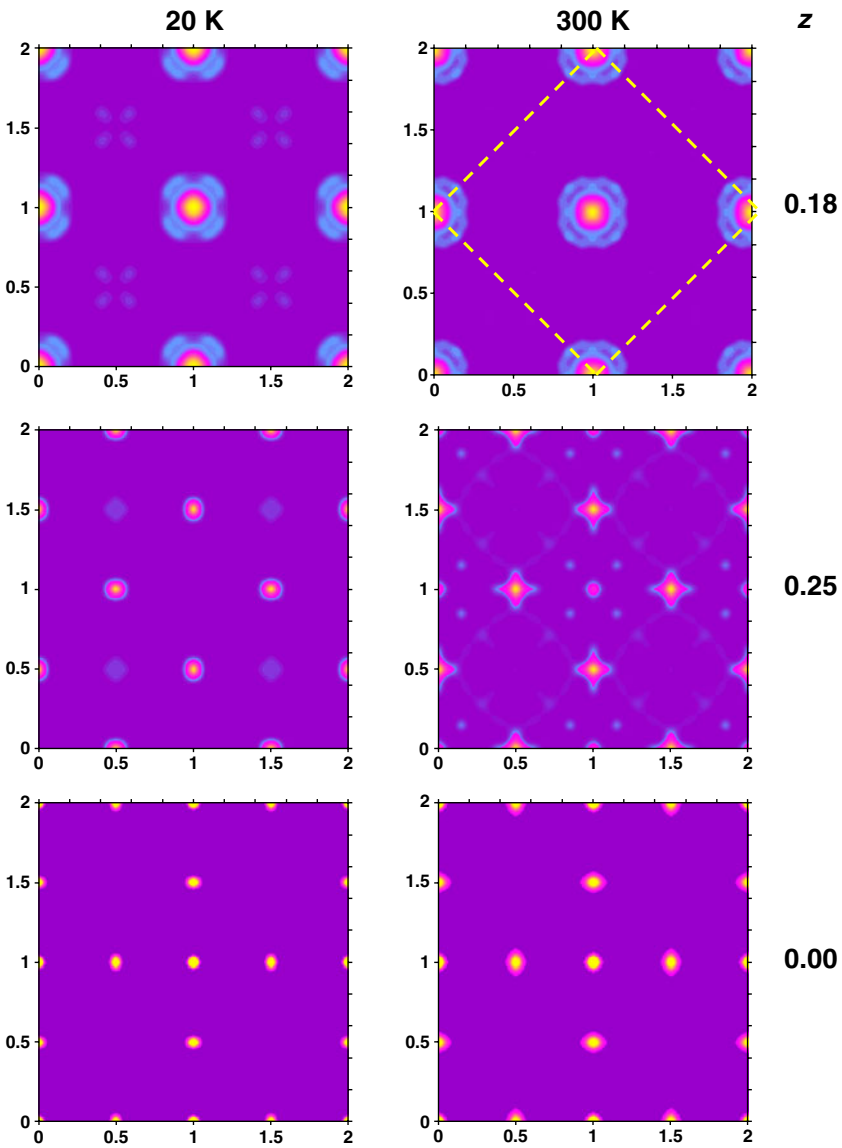


**Fig. 2** Nuclear scattering densities obtained from a $La_2CuO_{4.07}$ twinned single crystal by neutron diffraction studies and subsequent reconstruction using the maximum entropy method at 20 K and ambient temperature. Sections of the $CuO_2$ plane ($z$=0), the apical oxygen layer in $z$=0.18 and the interstitial oxygen section in $z$=0.25 are given. The $F$-centred unit cell is outlined for the figure at $z$=0.18 and 300 K

At 20 K, the interstitial oxygen atoms are on the defined (¼ ¼ ¼) position, related to the frozen arrangement of the symmetrically enlarged $O_{int}(O_{ap})_4$ tetrahedra. This scenario changes when switching to ambient temperature. Here, the tilting of the apical oxygen atoms in the [100] and [110] directions indicates an increase of the apical oxygen disorder, probably related to dynamic fluctuations as outlined below, and which also directly influences the displacements of the interstitial oxygen atoms. The nuclear density distribution of the latter atoms clearly indicates a distortion away from the (¼ ¼ ¼) position, which is a consequence of the tilting behaviour of the apical oxygen atoms and herein to maintain an approximate distance of 2.6 Å despite the $O_{ap}$ tilting.

This disorder scenario is different of the one found for $La_2NiO_{4+\delta}$ where a continuous decrease of the Debye–Waller factor of the $O_{int}$ was found with increasing temperature [4]. The decrease has been interpreted to be a consequence of the free libration mode of the $NiO_6$ octahedra, fully established at higher temperatures. Since these movements are much more restricted at lower temperatures, the increase of the $O_{int}$ displacement factors is thus a consequence of the repulsive interaction between the apical and interstitial oxygen atoms, which is, however, of more static origin. $La_2NiO_{4+\delta}$ is always tetragonal (or at least extremely close to a tetragonal symmetry) for $\delta$>0.02, and the tilting of the apical oxygen atoms is only observed in the [110] direction. For the $La_2MO_{4+\delta}$ (M=Cu, Co) series, the situation is different as the symmetry is always orthorhombic at ambient temperature for any $\delta$ value. In the case of $La_2CoO_{4+\delta}$, the $O_{ap}$ tilting direction depends mainly on $\delta$; for $0<\delta<0.1$ the tilting of the $O_{ap}$ is along [100], whilst for higher larger values of $\delta$, it deviates towards [110] [6].

The $O_{ap}/O_{int}$ interaction seems to be a critical point in the understanding of the low-temperature oxygen mobility mechanism. As a consequence of the disorder scheme described above and the lattice dynamical properties reported for $La_2CuO_4$, the disorder scenario may be interpreted to be—at least partially—a consequence of the tilt mode (soft mode) reported for $La_2NiO_4$ and $La_2CuO_4$ at the *X* point of the *I*4/*mmm* primitive Brillouin zone (Fig. 3). Phonon modes have been largely investigated in $K_2NiF_4$-type high-$T_C$ oxides with the aim of finding evidence for electron–phonon correlations. We want to stress here that phonon contributions might be considered as the key point to interpret the origin of oxygen mobility at moderate temperatures.

Structural correlations between apical and interstitial oxygen atoms and their impact for the diffusion pathway have been evidenced for different oxides with $RE_2NiO_4$ (RE = La, Pr)-type structure [4, 17–21].

It seems also obvious from structural considerations that the most obvious oxygen diffusion pathway in $K_2NiF_4$-type oxides is supposed to imply the move of apical oxygen atoms towards interstitial sites and vice versa. This kind of diffusion pathway was recently described to be present for $(Pr_{0.9}La_{0.1})_2(Ni_{0.74}Cu_{0.21}Ga_{0.05})O_{4+\delta}$ at elevated temperatures, as analysed from neutron powder diffraction data using the maximum entropy algorithm [18]. This type of vacancy diffusion mechanism was also simulated via molecular dynamics calculations to occur for oxygen-doped $La_2NiO_{4+\delta}$ and $Pr_2NiO_{4+\delta}$ phases on a picosecond timescale [20, 21], whilst it is interesting to note that in the same time window, no significant oxygen diffusion could be simulated for stoichiometric $La_2NiO_{4.00}$ by the same authors. However, these molecular dynamics simulations are based on Buckingham inter-ionic potential parameters that were fitted to reproduce the crystal structure, but not the shallow potential for apical oxygen.

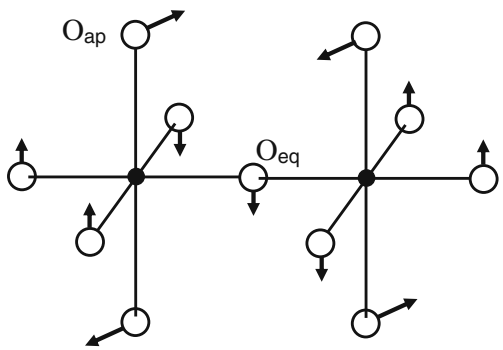


**Fig. 3** Lowest soft mode calculated for stoichiometric $La_2CuO_4$, corresponding to $MO_6$ tilt motions at the *X* point of the Brillouin zone for the pristine *I*4/*mmm* lattice. In $La_2CuO_{4+\delta}$, the lowest soft mode is of the same type, but the displacements of apical oxygen atoms neighbor to $O_{int}$ are quenched

The uptake of oxygen atoms into $K_2NiF_4$-type oxides results for $La_2MO_{4+\delta}$ (M = Cu, Ni, Co) into an average structure as outlined above. We want to stress that it remains still unclear today whether the related strong anisotropic displacement factors for the oxygen atoms are of dynamic origin or are a consequence of static displacements with an associated domain structure, averaging different tilting orientations of the $MO_6$ octahedra. This makes, however, a significant difference when exploring the origin of low-temperature oxygen diffusion. The importance of lattice dynamics for oxygen diffusion has been evidenced recently for $SrFeO_{2.5}$ with a Brownmillerite-type structure, resulting in a phonon-assisted diffusion model where oxygen atoms are able to diffuse along the underlying 1D vacancy channels via a dynamical switching mechanism of the $FeO_4$ tetrahedral chains. Free oxygen diffusion, i.e. without application of any external solicitation like an electrochemical potential, has been shown to be present in $SrFeO_{2.875}$ already above 300°C by $^{18}O/^{16}O$ isotope exchange experiments [7]. Given that lattice dynamics would also be at the origin of oxygen mobility in $K_2NiF_4$-type oxides, we would then expect a similar situation of specifically triggered lattice modes at low energy to be responsible for enhanced oxygen mobility. We have therefore investigated whether the strong anisotropic oxygen displacement factors, present at all temperatures, could be interpreted to have a dynamic origin and if these dynamics could explain and/or amplify diffusion from the apical to the interstitial vacancy sites. The other point is to investigate the influence of the interstitial oxygen atoms on oxygen mobility at low temperature and whether their presence is needed with respect to the stoichiometric compounds.

## Results and discussion: DFT calculations

DFT calculations have been performed for the undoped $La_2CuO_{4.00}$ using a *F*4/*mmm* tetragonal unit cell derived from the experimental structural data at room temperature (*Z*=4, Table 1): The *a* parameter of the tetragonal cell was taken as an average of the *a* and *b* parameters of the orthorhombic cell (Table 1). Subsequently, one interstitial oxygen atom per unit cell was introduced, corresponding to $La_2CuO_{4.25}$; as quoted above, the number of electrons was adjusted so as to correspond to $\delta$=1/16 in $La_2CuO_{4+\delta}$, a more realistic $\delta$ value for the $La_2CuO_{4+\delta}$ system. All atomic positions were relaxed in the $La_2CuO_{4.25}$ unit cell whilst keeping unit cell parameters fixed.

Table 2 displays selected bond lengths, mainly in the $La_2O_2$ rock salt layer containing $O_{int}$ and in the next $La_2O_2$ layer, free of interstitial species. The calculated $O_{ap}$–$O_{int}$ distance (2.55 Å) is in good agreement with the experimental value; within the $La_2O_{2+\delta}$ layer, a huge dimerization

**Table 2** Calculated bond lengths (in Å) in over-stoichiometric ($La_2O_{2+\delta}$) and $O_{int}$-free $La_2O_2$ layers, from the structural optimization of $La_2CuO_{4.25}$ at fixed unit cell parameters

| | $La_2CuO_{4.00}$ | $La_2CuO_{4.25}$ ($La_2O_{2+\delta}$ layer) | $La_2CuO_{4.25}$ ($O_{int}$-free layer) |
|---|---|---|---|
| La–$O_{ap}$ | 2.364 | 2.462 | 2.313 |
| | 2.735×4 | 2.394×2 | 2.673×2 |
| | | 3.035×2 | 2.835×2 |
| La–$O_{int}$ | | 2.362 | |
| $O_{ap}$–Cu | 2.417 | 2.310 | 2.492 |
| $O_{ap}$–$O_{ap}$ | 3.219×4 | 2.915×2 | 3.056×2 |
| | | 3.895×2 | 3.233×2 |
| | 3.81×4 | 2.899 | 3.634 |
| $O_{ap}$–$O_{int}$ | | 2.552 | |

Bond lengths for the idealized parent structure $La_2CuO_4$ (S. G. *F*4/*mmm*, see Table 1) are indicated for the sake of comparison

of both La–$O_{ap}$ and $O_{ap}$–$O_{ap}$ bonds occurs in the vicinity of $O_{int}$ (from 2.735 Å to 2.394 and 3.035 Å for La–$O_{ap}$, from 3.219 Å to 2.915 and 3.895 Å for $O_{ap}$–$O_{ap}$). These large distortions induce also a significant shortening of the $O_{ap}$–$O_{ap}$ distance (from 3.8 to 2.90 Å) of corner-sharing octahedra. La–$O_{int}$ is the shortest La–O bond, with a distance very close to La–$O_{ap}$ in the stoichiometric compound. In the next, $O_{int}$–free $La_2O_2$ layer, the modification of $O_{ap}$–$O_{ap}$ distances is less marked, indicating that the $O_{int}$–$O_{ap}$ steric repulsion does not lead to a rigid tilting of the $CuO_6$ octahedron. More generally, the crystal structure in $La_2O_2$ layers is perturbed in the same manner as in the $La_2O_{2+\delta}$ layer, but distortions are weaker. Besides, the octahedron distortion is associated with a significant dimerization of Cu–$O_{ap}$ bonds, from 2.417 Å in the stoichiometric compound to 2.310 and 2.492 Å. Zone-centre phonon modes were calculated for the $Z$=4 unit cell (Fig. 1) for the stoichiometric case and in the presence of one interstitial oxygen atom using in the latter case the relaxed atomic positions. As the chosen tetragonal unit cell contains four formula units and is face-centred, it allows describing phonons both at Γ and edge points of the Brillouin zone for the associated body-centred unit cell (*I*4/*mmm*, $Z$=2).

## Lattice dynamics of stoichiometric $La_2CuO_{4.00}$

Without $O_{int}$, the first nine optical modes are actual unstable modes (imaginary frequencies). Details are reported in Table 3. The mode of lowest energy corresponds to octahedra tilting (Fig. 3) at the $X$ point of the primitive Brillouin zone, as found for $La_2NiO_4$ [22]; however, the very negative value for $La_2CuO_4$ for this mode indicates a larger instability towards the orthorhombic distortion, in agreement with crystal structures at room temperature. This instability is probably more pronounced in $La_2CuO_4$ due to the Jahn–Teller distortion resulting in an increased Cu–$O_{ap}$ bond length of 2.40 Å compared to about 2.22 Å for the homologous Ni or Co compound. All unstable optical modes found here in $La_2CuO_{4.00}$, except the two rotational modes around −12.4 meV, involve large $O_{ap}$ displacements along the [100] or [010] direction, in particular for the bending modes at −12.1 and −11.3 meV and the tilting mode at −10.3 meV. La displacements in the *a,b* plane increase progressively with increasing phonon energies and become significant above −8 meV, whilst $O_{ap}$ displacements decrease conversely. The first ten optical modes of real frequency, up to 12.8 meV (3.1 THz), involve significant in-plane La and $O_{ap}$ displacements in the $La_2O_2$ layers, except two modes at 7.0 and 10.8 meV (1.68 and 2.62 THz).

Thus, most low-energy or soft modes in stoichiometric $La_2CuO_{4.00}$ involve significant $O_{ap}$ displacements in the [100] direction of the lattice. Some of these modes, associating appropriate in-plane lanthanum displacements, involve the breathing of the $La_2O_2$ windows connecting interstitial sites. Optical modes at −7.0, −5.4 and +10.6 meV correspond to out-of-phase breathing of $La_2O_2$ windows along the [100] or [010] direction; modes at 9.5, 11.2, 11.6 and 12.8 meV (2.30, 2.71, 2.80 and 3.10 THz) correspond to in-phase breathing of $La_2O_2$ windows. $La_2O_2$ windows breathing modes of low energy (shown in Fig. 4) might be correlated to, and facilitate, interstitial oxygen mobility along the [100] or [010] directions in $La_2CuO_{4+\delta}$ (direct hopping mechanism).

Push–pull mechanisms for interstitial oxygen mobility in $La_2CuO_4$-type lattices (preferential mechanism according to atomistic simulations) [19] involve coupled displacements of $O_{int}$ and neighbour $O_{ap}$. This mechanism can as well be facilitated by low-energy phonon modes found in $La_2CuO_4$, involving significant $O_{ap}$ displacements along the [100] or [010] direction.

Besides, one can track phonon modes with $O_{ap}$ displacements along the [110]-type directions, i.e. towards the interstitial site. We underline that such modes are found at much higher energies compared to O-intercalated $La_2CuO_{4+\delta}$. Only two modes with $O_{ap}$ displacements along [110] are found in stoichiometric $La_2CuO_{4.00}$, i.e. no. 39 and no. 40 (among 81 optical modes), at 19.7 and 20.9 meV (4.77 and 5.41 THz); these two modes involve mainly a buckling of the $CuO_2$ sheets along [100] and [010], coupled to quadrupolar $O_{ap}$–La displacements along [110]-type directions.

## Lattice dynamics of $La_2CuO_{4+\delta}$

When $O_{int}$ is included in the lattice, the phonon mode description is more complex due to the lower symmetry and

**Table 3** Frequencies ($f$), energies ($E$), distortion mode of the $O_{ap}$–Cu–$O_{ap}$ dumbbell and main atomic displacements for low-energy optical phonon modes in stoichiometric $La_2CuO_4$

| | | | | | | | | |
|---|---|---|---|---|---|---|---|---|
| $f$ (THz) | 3.99i | 3.02i/2.99i | 2.93i/2.74i | 2.53i | 2.48i | 1.70i | 1.30i | 1.23 |
| $E$ (meV) | −16.5 | −12.5/−12.3 | −12.1/−11.3 | −10.5 | −10.3 | −7.0 | −5.4 | 5.1 |
| $O_{ap}$–Cu–$O_{ap}$ | Tilting $CuO_6$ [100] | Rot $O_{eq}$ | Bending $La_2O_2$ [100] | Tilting La/$CuO_6$ [010] | Tilting $O_{ap}$ [100] | Bending $La_2O_2$ [100] | Tilting $La_2O_2$ [100] | Bending $La_2O_2$/y [010] |
| Phase | | | | | | Out-of-phase | Out-of-phase | |
| $f$ (THz) | 1.68 | 2.06/2.18 | 2.30 | 2.55 | 2.62 | 2.71 | 2.80 | 3.10 |
| $E$ (meV) | 7.0 | 8.5/9.0 | 9.5 | 10.6 | 10.8 | 11.2 | 11.6 | 12.8 |
| | La, $CuO_2$ [010] | Bending/tilting $La_2O_2$ [010]/[100] | Tilting $La_2O_2$ [010] | La [010] | La, $CuO_2$ [001] | Bending $La_2O_2$ [010] | Tilting $La_2O_2$ [100] | Bending $La_2O_2$ [100] |
| Phase | | | In-phase | Out-of-phase | | In-phase | In-phase | In-phase |

Phases for breathing modes of $La_2O_2$ windows (Fig. 4) are indicated

larger number of non-equivalent sites. In particular, $O_{int}$-free $La_2O_2$ layers behave clearly differently from $La_2O_{2+\delta}$ layers. Two general effects mainly emerge by the insertion of interstitial oxygen: (1) The structure is more rigid, leading to an overall shift towards higher phonon energies (higher frequencies); (2) [110]-type displacements for $O_{ap}$ are at lower energy, in agreement with the neutron diffraction data.

Four optical unstable modes are found, instead of nine, in the $O_{int}$-free structure. Three of them are remnants of the modes described above. In the fourth, the mode at −12.7 meV involves significant La and $O_{ap}$ movements along [100] in the $O_{int}$-free $La_2O_2$ layers only because the presence of $O_{int}$ prevents atomic displacements in the $La_2O_{2+\delta}$ layers. Thus, this mode becomes a deformation mode in the vicinity of $O_{int}$ instead of an actual octahedron tilting mode as for the undoped model. Two other soft modes (−7.0 and −3.65 meV) are related to $O_{eq}$ rotation modes found previously, mixed with modes of large $O_{ap}$ displacements along [100] that occur here in $O_{int}$-free $La_2O_2$ layers only. A fourth unstable mode is found at −4.13 meV; interestingly, it involves large La and $O_{ap}$ displacements along [110]-type directions in $O_{int}$-free $La_2O_2$ layers only, whereas such displacements were found at a significantly higher energy in the stoichiometric case.

Movements in over-stoichiometric $La_2O_{2+\delta}$ layers are progressively activated in modes of positive energy, but become significant only in high-energy optical modes (at 22.4 and 26.1 meV, for $O_{ap}$ and $O_{int}$, respectively). At moderate energies, these displacements are limited in magnitude and correspond to in-phase movements of $O_{int}$ and its first neighbours ($La_4O_5$ clusters) along [110]-type directions (modes in the range 3.27–9.74 meV or 0.79–2.35 THz).

The first phonon mode showing large $O_{ap}$ and La displacements in over-stoichiometric $La_2O_{2+\delta}$ layers lies at 14.2 meV (3.44 THz). These displacements are along [110]-type directions and corresponds to La–$O_{ap}$ quadrupolar vibrations.

Modes associated to breathing of $La_2O_2$ windows connecting interstitial sites are found at higher energies than in the stoichiometric case, especially for out-of-phase modes that lie at 12.4 meV (2.99 THz) and 13.2 meV (3.20 THz, Fig. 4); the latter is the first optical mode involving $La_2O_{2+\delta}$ layers. In-phase opening of $La_2O_2$ windows ($La_2O_2$ layers only) is found for modes at 11.9 meV (2.89 THz) and 13.8 meV (3.33 THz). Further details on the energy mode at the $X$ point are listed in Table 4.

In conclusion, $O_{int}$ has a stiffening effect on the lattice dynamics, especially in $O_{int}$-containing layers. $La_2O_2$ windows breathing modes, which can contribute to oxygen migration via direct hopping between interstitial sites, are clearly shifted to higher frequencies by $O_{int}$. On the other side, the presence of interstitial oxygen activates significantly La/$O_{ap}$ displacements along [110]-type directions, even at low energies; this kind of vibrations might be an enhancing factor for push–pull migration mechanisms [19], especially at moderate temperatures. The found distortions go along with the oxygen diffusion pathway experimentally evidenced for $(La,Pr)_2(Ni,Cu,Ga)O_{4+\delta}$ at 1015 °C [18], which is also somehow identical with what has been simulated for $La_2NiO_{4+\delta}$ [20] above 800 K. It is worth mentioning that our findings already concern importantly the temperature regime of 300 K.

## Concluding remarks

The experimentally evidenced [110] displacements (see Fig. 3) of the apical oxygen atoms in $La_2CuO_{4.07}$ by single-crystal neutron diffraction at 300 K were confirmed and found to occur already at low energy (−4.1 meV) by first-principles calculations. The same type of lattice modes is

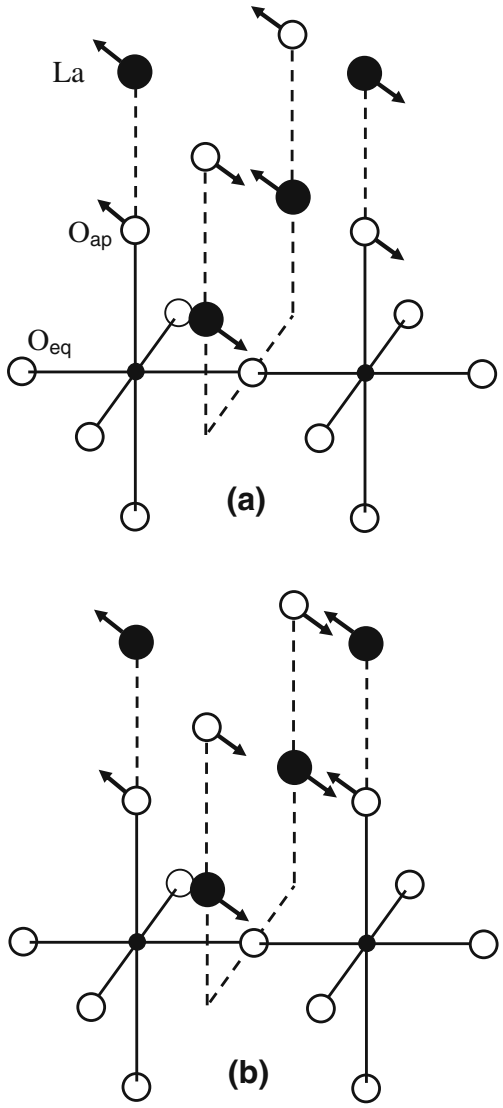


**Fig. 4** Breathing modes of $La_2O_2$ windows connecting interstitial sites: in-phase (**a**) and out-of-phase (**b**)

found at a much higher energy (20 meV) in stoichiometric $La_2CuO_{4.00}$. The simultaneous displacements towards [110] and [100] in the oxygen-doped $La_2CuO_{4.07}$ found to be present already at room temperature are equivalent to a dynamic displacement of the apical oxygen on a circle of about 0.5 Å in radius around its average position, in accordance with a tilt angle of the $CuO_6$ octahedra of about 12°. The strong displacements of the apical oxygen are also coherent with a $O_{ap}$–$O_{int}$ distance of about 2.58 Å, confirming the valence state of $O_{int}$ to be −2. Similar values have already been obtained for $La_2NiO_{4+\delta}$ [4, 17].

Following the details of the DFT calculations, the modes observed for stoichiometric and doped $La_2CuO_{4+\delta}$ are significantly different. To interpret straightforwardly these modes, we first focus on the comparison of displacements in the $O_{int}$-free $La_2O_2$ and $La_2O_{2+\delta}$ units (layers) in terms of energy and directions. As for the undoped $La_2CuO_{4.00}$, modes towards [110] were simulated above 20 meV only, whereas the same modes occur for the oxygen-doped system already at negative energies. This underpins the concept of the local instability of the apical oxygen atoms to be more pronounced in doped $La_2CuO_{4+\delta}$. In the latter, a more detailed inspection shows that the modes for the over-stoichiometric $La_2O_{2+\delta}$ units are situated at much higher energies compared to $O_{int}$-free $La_2O_2$ units, revealing two important differences. The first is that the dynamical [110] shifts of the apical oxygen atoms of the $O_{int}$-free $La_2O_2$ units are much more easily activated, allowing the apical oxygen atoms to get displaced towards the interstitial vacancy sites in a facile way. On the other hand, the interstitial oxygen atoms in an over-stoichiometric $La_2O_{2+\delta}$ unit induce a local stiffening of the lattice, involving the important consequence that the mobile oxygen species are probably not the interstitial oxygen atoms directly, but the apical oxygen of any $O_{int}$-free $La_2O_2$ unit, at least from the lattice dynamics point of view. This yields a difference in the diffusion mechanism on a microscopic scale as, intuitively, one would assume the diffusion of the interstitial oxygen atoms to be predominant. Consequently, it becomes then clear that the presence of the interstitial oxygen

**Table 4** Frequencies (*f*), energies (*E*) and main atomic displacements for low-energy optical phonon modes in $La_2CuO_{4+\delta}$

| | | | | | | | | |
|---|---|---|---|---|---|---|---|---|
| *f* (THz) | 3.06i | 1.69i/0.88i | 1.00i | 0.79 | 1.47 | 1.97 | 2.08 | 2.22/2.35 |
| *E* (meV) | −12.7 | −7.0/−3.6 | −4.1 | 3.3 | 6.1 | 8.1 | 8.6 | 9.2/9.7 |
| | Semi-tilt. $O_{eq}$, $La_2O_2$ [100] | Rot $O_{eq}$ $La_2O_2$: [100] | $La_2O_2$ [110], [010] | $La_2O_2$,$CuO_2$ [100] | Rot $O_{eq}$ $O_{ap}$: [100] La: [110] | Cu, La [010] | $CuO_2$ [001] | La, $CuO_2$ [110] |
| *f* (THz) | 2.89 | 2.99 | 3.10 | 3.20 | 3.33 | 3.36/3.42 | 3.44 | 3.61 |
| *E* (meV) | 11.9 | 12.4 | 12.8 | 13.2 | 13.8 | 13.9/14.2 | 14.2 | 14.9 |
| | $CuO_2$: [001] $La_2O_2$: [010] | La, $CuO_2$ [100] | $CuO_2$: [001] $La_2O_2$: [110] | La [010] | $La_2O_2$ [100] | Cu, La [001] | Quadrup. $La_2O_{2+\delta}$ [110] | Cu, La, $O_{int}$ [001] |
| Phase | In-phase | Out-of-phase | | Out-of-phase | In-phase | | | |

Phases for breathing modes of $La_2O_2$ windows (Fig. 4) are indicated

atoms importantly favours the diffusion of the oxygen atoms of the $O_{int}$-free $La_2O_2$ units from the apical to interstitial lattice sites due to a considerably modified lattice dynamics; this mechanism may compete with the push–pull mechanism in over-stoichiometric $La_2O_{2+\delta}$ layers in which large $O_{int}$-induced local strain weakens the Cu–$O_{ap}$ bond but also prevents low-energy phonon modes.

We may then consider low-temperature oxygen diffusion to be mainly induced by lattice dynamical aspects, associated with lattice instabilities. In this way, the mechanism of oxygen intercalation into $K_2NiF_4$-type oxides has to be considered to proceed on a similar microscopic scheme as found for Sr(Fe, Co)$O_{2.5}$ with Brownmillerite-type structure, i.e. essentially activated via specific low-energy lattice modes, allowing a phonon-assisted diffusion. This is with respect to its origin different from the classical push–pull mechanism activated at higher temperatures, which has a more isotropic character, following the Arrhenius ansatz.

**Acknowledgements** This work was supported by the project FUSTOM delivered from the French National Research Agency (ANR-08-BLAN-0069). L.LD. was supported by a BDI-PhD grant, provided by the CNRS (France) and the ESM Foundation (Switzerland). M.I.H. is grateful for a French-Tunisian PhD grant.

## References

1. Wattiaux A, Fournès L, Demourges A, Bernaben N, Grenier JC, Pouchard M (1991) Solid State Commun 77:489
2. Bezdicka P, Wattiaux A, Grenier JC, Pouchard M, Hagenmuller P (1993) Z Anorg Allg Chem 619:7
3. Le Toquin R, Paulus W, Cousson A, Prestipino C, Lamberti C (2006) J Am Chem Soc 128:13161
4. Paulus W, Cousson A, Dhalenne G, Berthon J, Revcolevschi A, Hosoya S, Treutmann W, Heger G, Le Toquin R (2002) Solid State Sci 4:565
5. Paulus W, Heger G, Rudolph P, Schöllhorn R (1994) Phys C 235–240:861
6. Le Toquin R, Paulus W, Cousson A, Dhalenne G, Revcolevschi A (2004) Phys B 350:e269
7. Paulus W, Schober H, Eibl S, Johnson M, Berthier T, Hernandez O, Ceretti M, Plazanet M, Conder K, Lamberti C (2008) J Am Chem Soc 130:16080
8. Lee CH, Kaneko N, Hosoya S, Kurahashi K, Wakimoto S, Yamada K, Endoh Y (1998) Supercond Sci Technol 11:891
9. Scheldrick GM. SHELX-97. University of Göttingen, Germany.
10. Kumazawa S, Kubota Y, Takata M, Sakata M (1993) J Appl Crystallogr 26:453
11. Koester L, Rauch H, Seymann E (1991) At Data Nucl Data Tables 49:65
12. Kresse G, Hafner J (1996) Comput Mater Sci 6:15. http://cms.mpi.univie.ac.at/vasp
13. Kresse G, Furthmüller J (1996) Phys Rev B 54:11169
14. Kresse G, Hafner J (1993) Phys Rev B 47:RC558
15. Perdew JP, Burke K, Ernzerhof M (1996) Phys Rev Lett 77:3865
16. Lee KH, Hoffmann R (2006) J Phys Chem A 110:609
17. Frayret C, Villesuzanne A, Pouchard M (2005) Chem Mater 17:6358
18. Yashima M, Enoki E, Wakita T, Ali R, Matsushita Y, Izumi F, Ishihara T (2008) J Am Chem Soc 130:2762
19. Minervini L, Grimes RW, Kilner JA, Sickafus KE (2000) J Mater Chem 10:2349
20. Chroneos A, Parfitt D, Kilner JA, Grimes RW (2010) J Mater Chem 20:266
21. Parfitt D, Chroneos A, Kilner JA, Grimes RW (2010) Phys Chem Chem Phys 12:6834
22. Pintschovius L, Bassat JM, Odier P, Gervais F, Chevrier G, Reichardt W, Gompf F (1989) Phys Rev B 40:2229